

ARTICLE

Received 9 Jan 2012 | Accepted 23 Apr 2012 | Published 22 May 2012

DOI:10.1038/ncomms1856

Suppression of spin-bath dynamics for improved coherence of multi-spin-qubit systems

N. Bar-Gill^{1,2}, L.M. Pham³, C. Belthangady¹, D. Le Sage¹, P. Cappellaro⁴, J.R. Maze⁵, M.D. Lukin², A. Yacoby² & R. Walsworth^{1,2}

Multi-qubit systems are crucial for the advancement and application of quantum science. Such systems require maintaining long coherence times while increasing the number of qubits available for coherent manipulation. For solid-state spin systems, qubit coherence is closely related to fundamental questions of many-body spin dynamics. Here we apply a coherent spectroscopic technique to characterize the dynamics of the composite solid-state spin environment of nitrogen-vacancy colour centres in room temperature diamond. We identify a possible new mechanism in diamond for suppression of electronic spin-bath dynamics in the presence of a nuclear spin bath of sufficient concentration. This suppression enhances the efficacy of dynamical decoupling techniques, resulting in increased coherence times for multi-spin-qubit systems, thus paving the way for applications in quantum information, sensing and metrology.

¹ Harvard-Smithsonian Center for Astrophysics, Cambridge, Massachusetts 02138, USA. ² Department of Physics, Harvard University, Cambridge, Massachusetts 02138, USA. ³ School of Engineering and Applied Sciences, Harvard University, Cambridge, Massachusetts 02138, USA. ⁴ Department of Nuclear Science and Engineering, MIT, Cambridge, Massachusetts 02139, USA. ⁵ Department of Physics, Pontificia Universidad Catolica de Chile, Santiago 7820436, Chile. Correspondence and requests for materials should be addressed to N.B.G. (email: nbar-gill@cfa.harvard.edu) or to R.W. (email: rwalsworth@cfa.harvard.edu).

Understanding and controlling the coherence of multi-spin-qubit solid-state systems is crucial for quantum information science^{1–3}, basic research on quantum many-body dynamics⁴ and quantum sensing and metrology^{5–9}. Examples of such systems include nitrogen-vacancy (NV) colour centres in diamond¹⁰, phosphorous donors in silicon¹¹ and quantum dots¹². In characterizing the potential usefulness of multi-qubit systems for quantum applications, the product of the qubit density (n_{qb}) and the qubit coherence lifetime (T_2) serves as a basic figure-of-merit (FOM), $\text{FOM} = n_{\text{qb}} T_2$. For example, in quantum measurements the phase-shift sensitivity $\delta\phi$ scales as $1/\sqrt{\text{FOM}}$ ^{5,13–15}. Increasing this multi-qubit FOM requires an understanding of the sources of decoherence in the system and their interplay with qubit density. In particular, for solid-state spin qubits T_2 is typically limited by interaction with an environment (that is, bath) of paramagnetic spin impurities, whereas n_{qb} is limited by fabrication issues, the associated creation of additional spin impurities in the environment, and the ability to polarize (state prepare) the quantum spins.

The paradigm of a central spin coupled to a spin environment has been studied intensively for many years (see for example refs 16 and 17), and quantum control methods have been developed to extend the spin coherence lifetime by reducing the effective interaction with the environment. In particular, dynamical decoupling techniques pioneered in nuclear magnetic resonance have recently been applied successfully to extend the effective T_2 of single NV-diamond electronic spins by more than an order of magnitude^{18–20}.

Here we study experimentally the spin environment of NV colour centres in room temperature diamond and their multi-spin-qubit FOM. We apply a spectral decomposition technique^{21–23} to characterize the dynamics of the composite solid-state spin bath, consisting of both electronic spin (N) and nuclear spin (^{13}C) impurities. We study three different diamond samples with a wide range of NV densities and impurity spin concentrations (measuring both NV ensembles and single NV centres), and find unexpectedly long correlation times for the electronic spin baths in two diamond samples with natural abundance (1.1%) of ^{13}C nuclear spin impurities. We identify a possible new mechanism in diamond involving an interplay between the electronic and nuclear spin baths that can explain the observed suppression of electronic spin-bath dynamics. We show that this spin-bath suppression enhances the efficacy of dynamical decoupling techniques, enabling large values for the multi-qubit FOM $\sim 2 \times 10^{14}$ (ms cm^{−3}; compare, for example, to ref. 24, and to the similar FOM obtained with a much higher NV density sample⁹).

Results

Spectral decomposition technique. Owing to coupling of the NV spins to their magnetic environment (Fig. 1a,b), coherence is lost over time with the general form $C(t) = e^{-\chi(t)}$, where the functional $\chi(t)$ describes the time dependence of the decoherence process (Supplementary Methods). In the presence of a modulation acting on the NV spins (for example, a resonant MW (microwave) pulse sequence), described by a filter function in the frequency domain $F_t(\omega)$ (see below), the decoherence functional is given by^{25,26},

$$\chi(t) = \frac{1}{\pi} \int_0^\infty d\omega S(\omega) \frac{F_t(\omega)}{\omega^2}, \quad (1)$$

where $S(\omega)$ is the spectral function describing the coupling of the system to the environment. Equation (1) holds in the approximation of weak coupling of the NV spins to the environment, which is appropriate for systems with (dominantly) electronic spin baths¹⁷, as is the case with the diamond samples discussed here (see below).

$S(\omega)$ can be determined from straightforward decoherence measurements of the NV spin qubits using a spectral decomposition

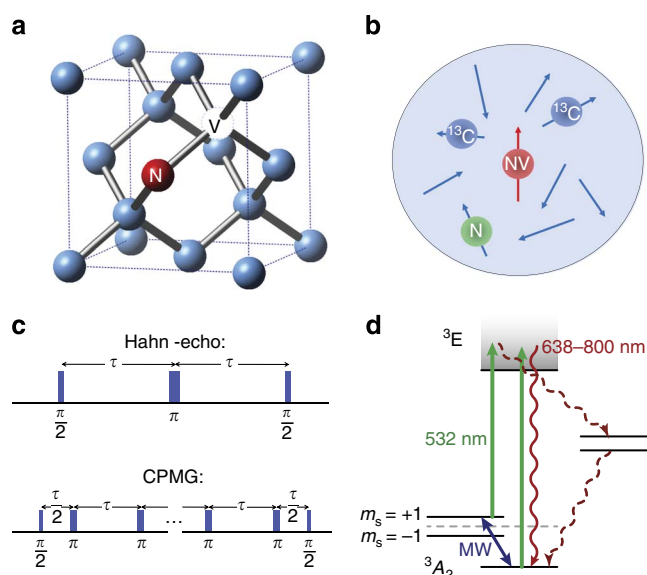


Figure 1 | NV centre in diamond and applied spin-control pulse sequences. (a) Lattice structure of diamond with an NV colour centre.

The NV electronic spin axis is defined by nitrogen and vacancy sites, in one of four crystallographic directions in the diamond lattice. NV orientation subsets can be spectrally selected by applying a static magnetic field B_0 . (b) Magnetic environment of NV centre electronic spin: ^{13}C nuclear spin impurities and N electronic spin impurities. (c) Hahn-echo and multi-pulse (CPMG) spin-control sequences. (d) Negatively charged NV centre electronic energy level structure. Electronic spin polarization and readout is performed by optical excitation at 532 nm and red fluorescence detection. Ground-state spin manipulation is achieved by resonant MW excitation. The ground-state triplet has a zero magnetic field splitting ≈ 2.87 GHz.

technique^{21–23}. As seen from equation (1), if an appropriate modulation is applied to the NV spins such that $F_t(\omega)/(\omega^2 t) = \delta(\omega - \omega_0)$, that is, if a Dirac δ -function is localized at a desired frequency ω_0 , then $\chi(t) = tS(\omega_0)/\pi$. Therefore, by measuring the time dependence of the qubit coherence $C(t)$ when subjected to such a spectral δ -function modulation, we can extract the spin bath's spectral component at frequency ω_0 :

$$S(\omega_0) = -\pi \ln(C(t))/t. \quad (2)$$

This procedure can then be repeated for different values of ω_0 to provide complete spectral decomposition of the spin environment.

A close approximation to the ideal spectral filter function $F_t(\omega)$ described above can be provided by a variation on the well-known Carr–Purcell–Meiboom–Gill (CPMG) pulse sequence for dynamical decoupling of a qubit from its environment²⁷ (Fig. 1c). The CPMG pulse sequence is an extension of the Hahn-echo sequence²⁸ (Fig. 1c), with n equally spaced π -pulses applied to the system after initially rotating it into the x axis with a $\pi/2$ -pulse. We apply a deconvolution procedure to correct for deviations of this filter function from the ideal Dirac δ -function (Supplementary Fig. S1 and Supplementary Methods).

Spectral function of a spin bath. The composite solid-state spin environment in diamond is dominated by a bath of fluctuating N electronic spin ($S = 1/2$) impurities, which causes decoherence of the probed NV electron-spin qubits through magnetic dipolar interactions. In the regime of low external magnetic fields and room temperature (relevant to the present experiments), the N bath spins

are randomly oriented, and their flip-flops (spin-state exchanges) can be considered as random uncorrelated events¹⁷. Therefore, the resulting spectrum of the N bath's coupling to the NV spins can be assumed to be Lorentzian²⁵:

$$S(\omega) = \frac{\Delta^2 \tau_c}{\pi} \frac{1}{1 + (\omega \tau_c)^2}. \quad (3)$$

This spin-bath spectrum is characterized by two parameters: Δ is the average coupling strength of the N bath to the probed NV spins, and τ_c is the correlation time of the N bath spins with each other, which is related to their characteristic flip-flop time. In general, the coupling strength Δ is given by the average dipolar interaction energy between the bath spins and the NV spins, and the correlation time τ_c is given by the inverse of the dipolar interaction energy between neighbouring bath-spins. As such spin-spin interactions scale as $1/r^3$, where r is the distance between spins, it is expected that the coupling strength scales as the N bath spin density n_{spin} (that is, $\Delta \propto n_{\text{spin}}$), and the correlation time scales as the inverse of this density (that is, $\tau_c \propto n_{\text{spin}}$).

Note also that the multi-pulse CPMG sequence used in the spectral decomposition technique extends the NV spin coherence lifetime by suppressing the time-averaged coupling to the fluctuating spin environment. In general, the coherence lifetime T_2 increases with the number of pulses n used in the CPMG sequence. For a Lorentzian bath, in the limit of very short correlation times ($\tau_c \ll T_2$), the sequence is inefficient and $T_2 \propto n^0$ (no improvement with number of pulses). In the opposite limit of very long correlation times $\tau_c \gg T_2$, the scaling is $T_2 \propto n^{2/3}$ (refs 29–31; see also recent work on quantum dots³²). In the following we apply spectral decomposition to study the spin-bath dynamics and resulting scaling of T_2 with n for NV centres in diamond.

Experimental application of spectral decomposition. The NV centre is composed of a substitutional nitrogen atom and a vacancy on adjacent lattice sites (Fig. 1a). The negatively charged state, which is the focus of this work, is believed to gain an electron from nearby nitrogen donor impurities. The energy-level diagram of an NV centre is depicted in Fig. 1d. The NV centre has an electronic spin-triplet ground state with a zero-magnetic-field splitting ≈ 2.87 GHz between the $m_s = 0$ and $m_s = \pm 1$ spin states, quantized along the NV axis. A small external magnetic field applied along this axis lifts the degeneracy of the $m_s = \pm 1$ energy levels with a Zeeman shift ≈ 2.8 MHz G⁻¹. Optical transitions between the electronic ground and excited states have a characteristic zero-phonon line at 637 nm, although 532-nm light is typically used to drive excitation to a phonon-sideband, and NV centres fluoresce at room temperature over a broad range of wavelengths that is roughly peaked around 700 nm. Optical cycling transitions between the ground and excited states are primarily spin conserving. However, there exists a decay path that preferentially transfers the $m_s = \pm 1$ excited state population to the $m_s = 0$ ground-state through a metastable singlet state, without emitting a photon in the fluorescence band. It is this decay channel that allows the NV centre's spin-state to be determined from the fluorescence signal, and also leads to optical pumping into the $m_s = 0$ ground-state.

Experimentally, we manipulate the $|0\rangle - |1\rangle$ spin manifold of the NV triplet electronic ground state using a static magnetic field and resonant MW pulses, and use a 532-nm laser to initialize and provide optical readout of the NV spin states (Fig. 1d). More specifically, we optically initialize the NV spins to $m_s = 0$, apply CPMG pulse sequences (Fig. 1c) with varying numbers of π -pulses n and varying free precession times τ , and then measure the NV spin state using optical readout to determine the remaining NV multi-spin coherence (for details see the Methods and refs 13,14,10).

Table 1 | Comparison of key characteristics and extracted 'average-fit' Lorentzian spin-bath parameters for the NV-diamond samples studied in this work.

	¹² C	Apollo	HPHT
Measured technique	Wide field	Wide field	Confocal
N Concentration, p.p.m.	~1	~100	~50
NV density, cm ⁻³	~10 ¹⁴	~10 ¹⁶	~10 ¹²
¹³ C Concentration, %	0.01	1.1	1.1
Echo (1-pulse) T_2 , μ s	240 (6)	2 (1)	5 (1)
T_2 scaling	$\eta^{0.43(6)}$	$\eta^{0.65(5)}$	$\eta^{0.7(1)}$
Max. achieved T_2 , μ s	2.2	20	35
Δ (expected)	≈ 60 kHz	≈ 6 MHz	≈ 3 MHz
Δ (measured)	30 (10) kHz	7 (3) MHz	1 (1) MHz
τ_c (expected), μ s	≈ 15	≈ 0.17	≈ 0.34
τ_c (measured), μ s	10 (5)	3 (2)	10 (5)
FOM (ms cm ⁻³)	2×10^{14}	2×10^{14}	10^{10}

The measured coherence is then used to extract the corresponding spin-bath spectral component $S_n(\omega)$ as described above.

We applied the spectral decomposition technique to extract the spin-bath parameters Δ and τ_c as well as the NV multi-qubit coherence T_2 and FOM for three diamond samples with differing NV densities and concentrations of electronic and nuclear spin impurities (Table 1). The first sample, referred to as the ¹²C sample, is an isotopically pure ¹²C diamond sample grown by chemical vapour deposition (Element 6), which we studied using an NV wide-field microscope¹³. This sample has a very low concentration of ¹³C nuclear spin impurities (0.01%), a moderate concentration of N electronic spin impurities (~1 p.p.m.), and a moderate NV density (~10¹⁴ cm⁻³). We then measured the Apollo sample, a chemical vapour deposition diamond sample with a thin N-doped layer with natural ¹³C concentration (1.1%), high N concentration (~100 p.p.m.), and large NV density (~10¹⁶ cm⁻³), which we also studied using the NV wide-field microscope. The last sample, referred to as the high-pressure high-temperature (HPHT) sample, is a type 1b HPHT diamond sample (Element 6) with natural ¹³C concentration, high N concentration (~50 p.p.m.) and low NV density (~10¹² cm⁻³), which we observed under a confocal microscope able to measure single NV centres.

The results for the ¹²C sample are summarized in Fig. 2. In Fig. 2a we plot examples of the measured NV multi-spin coherence decay $C_n(t)$ as a function of pulse sequence duration t for CPMG pulse sequences with different numbers of π -pulses n . The measured $C_n(t)$ are well described by a stretched exponential $e^{-(t/T_2)^p}$, which is consistent with an electronic spin bath described by a Lorentzian spectrum (Supplementary Methods). We analysed such NV decoherence data using the spectral decomposition technique outlined above to extract the best-fit Lorentzian spin-bath spectrum (fit to the average of all data points), yielding a coupling strength of $\Delta = 30 \pm 10$ kHz and correlation time $\tau_c = 10 \pm 5$ μ s, which agrees well with the range of values we find for the Lorentzian spin-bath spectra $S_n(\omega)$ fit to each CPMG pulse sequence individually, $\Delta \approx 30$ to 50 kHz and $\tau_c \approx 5$ to 15 μ s (Fig. 2b, see Methods). These values are in reasonable agreement with the expected 'N dominated bath' values for Δ and τ_c for this sample's estimated concentrations of ¹³C and N spins (Table 1), indicating that N electronic spin impurities are the dominant source of NV decoherence. In Fig. 2c we plot the NV multi-spin coherence lifetime T_2 , determined from the measured coherence decay $C_n(t)$, as a function of the number n of CPMG π -pulses.

We repeated the spectral decomposition analysis for the two other diamond samples, with the results for all three samples summarized in Fig. 3 and Table 1. We find reasonable agreement between the measured and expected values for the NV/spin-bath

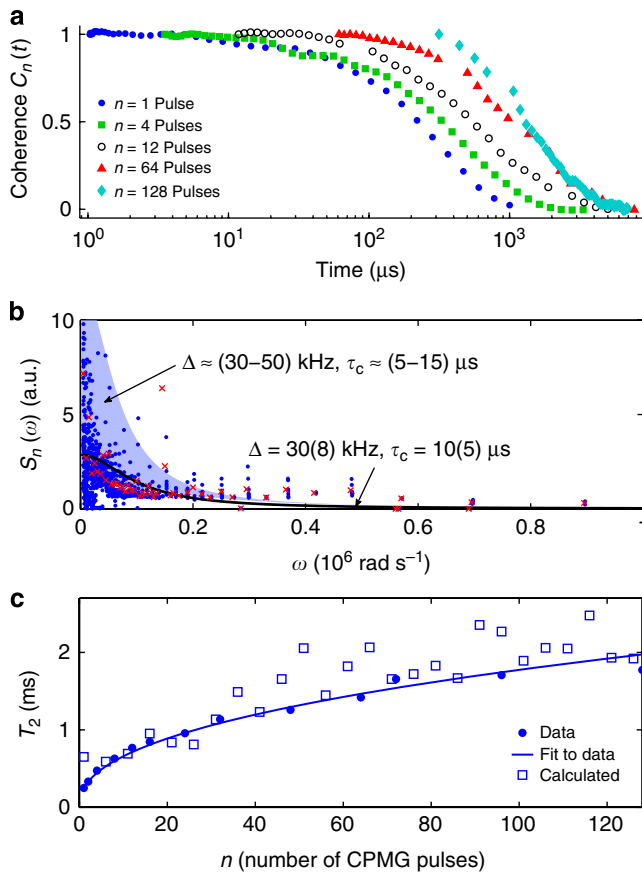


Figure 2 | Application of the spectral decomposition technique to an isotopically pure ^{12}C NV-diamond sample. (a) Examples of measured NV multi-spin coherence as a function of time $C_n(t)$ for CPMG pulse sequences with different numbers of pulses n . (b) Derived values for the spin-bath spectral functions $S_n(\omega)$ for all CPMG pulse sequences (blue dots) and average values at each frequency (red crosses). Each blue dot represents a pulse sequence with a specific duration t and number of pulses n , such that the probed frequency is $\omega = \pi n/t$. Also shown is the best-fit Lorentzian for the mean spectral function $\langle S_n(\omega) \rangle_n$ (solid black line), and a range of best-fit Lorentzians for the individual spectral functions $S_n(\omega)$ for each CPMG pulse sequence (light-blue band); a.u., arbitrary unit. (c) Scaling of T_2 with the number n of CPMG pulses: derived from NV spin coherence decay data $C_n(t)$ (dots); fit of data to a power law $T_2 = 250(40) \mu\text{s} \times n^{0.43(6)}$ (solid line); and synthesized from the average-fit Lorentzian spin-bath spectrum with $\Delta = 30 \text{ kHz}$, $\tau_c = 10 \mu\text{s}$ (open squares), which yields a consistent fit $T_2 = 270(100) \mu\text{s} \times n^{0.4(1)}$.

coupling strength Δ in all three NV-diamond samples, with Δ scaling approximately linearly with the N concentration. As mentioned before, the measured and expected values for the spin-bath correlation time τ_c agree well for the ^{12}C sample. However, we find a striking discrepancy between the measured and expected values of τ_c for the two samples with 1.1% ^{13}C concentration (Apollo and HPHT): both samples have measured spin-bath correlation times that are more than an order of magnitude longer than that given by the simple electronic spin-bath model, although the relative values of τ_c for these two samples scale inversely with N concentration, as expected.

Discussion

We explain this suppression of spin-bath dynamics as a result of random, relative detuning of electronic spin energy levels due to interactions between proximal electronic (N) and nuclear (^{13}C)

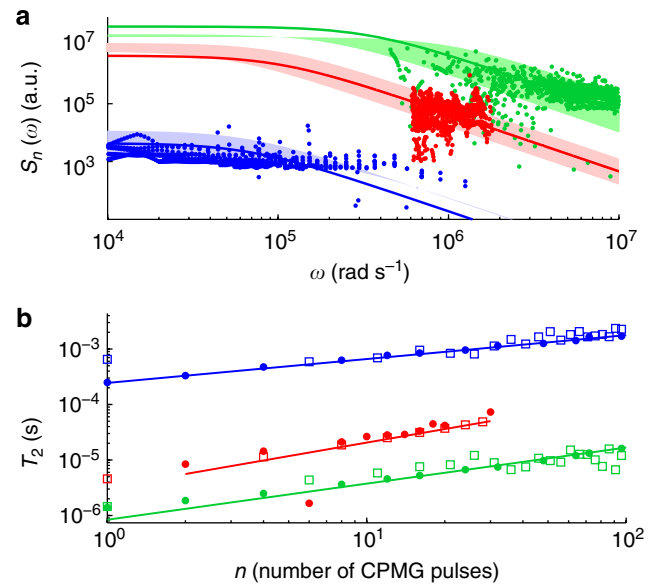


Figure 3 | Comparative application of the spectral decomposition technique to the ^{12}C (blue), Apollo (green) and HPHT (red) NV-diamond samples. (a) Spin-bath spectral functions data for all CPMG pulse sequences (dots), and associated Lorentzian fits using the average-fit method (solid lines) and the individual-fit method (colour bands); a.u., arbitrary unit. (b) Scaling of T_2 with the number of CPMG pulses n : derived from NV spin coherence decay data $C_n(t)$ (dots); fit of dots to a power law (solid lines); and synthesized from the average-fit Lorentzian spin-bath spectrum (open squares). The fitted scalings are: $T_2 \propto n^{0.43(6)}$ (^{12}C), $T_2 \propto n^{0.65(5)}$ (Apollo), $T_2 \propto n^{0.7(1)}$ (HPHT).

spin impurities (similar to processes identified by Bloembergen³³ and Portis³⁴ for other solid-state spin systems). The ensemble average effect of such random electronic-nuclear spin interactions is to induce an inhomogeneous broadening ΔE of the resonant electronic spin transitions in the bath, which reduces the electronic spin flip-flop rate R ($\sim 1/\tau_c$) given by^{35,36}

$$R \propto \frac{\pi \Delta_N^2}{9 \Delta E}, \quad (4)$$

where Δ_N is the dipolar interaction between N electronic spins. In this physical picture, ΔE is proportional to the concentration of ^{13}C impurities and to the N- ^{13}C hyperfine interaction energy, whereas Δ_N is proportional to the N concentration. Given the magnetic moments and concentrations of the N and ^{13}C spin impurities, and the large N- ^{13}C hyperfine interaction in diamond^{37,38}, we estimate $\Delta E \sim 10 \text{ MHz}$ and $\Delta_N \sim 1 \text{ MHz}$ for the Apollo and HPHT samples. These values imply an order of magnitude suppression of R compared with the bare electronic spin flip-flop rate ignoring N- ^{13}C interactions ($R_{\text{bare}} \sim \Delta_N$), which is consistent with our experimental results for $\tau_c \sim 1/R$ (Table 1). The estimate of ΔE is based on a Monte-Carlo simulation of the relative hyperfine interactions of 1,000 N spin pairs with a random distribution of ^{13}C spin impurities at the natural abundance concentration of 1.1% (Supplementary Methods). For the ^{12}C sample, the low concentration of ^{13}C spins greatly reduces the magnitude of ΔE , and hence the spin-bath suppression is negligible.

Importantly, we found large values for the multi-qubit FOM $\sim 2 \times 10^{14} (\text{ms cm}^{-3})$ for both the ^{12}C and Apollo samples. (The HPHT sample has a relatively low FOM, as expected given its low NV density.) The long coherence time obtained for the Apollo sample, with high NV density, natural 1.1% ^{13}C abundance and large N concentration,

is a result of the combined effect of suppression of electronic spin-bath dynamics and dynamical decoupling: the extended spin-bath correlation time enhances the effectiveness of dynamical decoupling, such that T_2 is increased by a factor of ~ 10 despite the large concentration of N impurities (which would naively suggest almost no dynamic decoupling improvement of T_2 for this sample³⁰).

In summary, we applied the spectral decomposition technique to three NV-diamond samples with different composite-spin environments to characterize the spin-bath dynamics and determine the NV multi-spin-qubit FOM. For samples with a finite concentration of ^{13}C nuclear spin impurities, this technique revealed an order-of-magnitude suppression of the N electronic spin-bath dynamics, which can be explained by random interactions between proximal electronic and ^{13}C nuclear spin impurities. This spin-bath suppression enhances the efficacy of dynamical decoupling for samples with high N impurity concentration, enabling increased NV spin coherence times and thus realization of a FOM $\sim 2 \times 10^{14}$ (ms cm^{-3}), which is within an order of magnitude of the state-of-the-art spin coherence FOM achieved in atomic systems¹⁵. Further optimization of the multi-spin-qubit FOM may be possible by engineering this spin-bath suppression, for example, with ^{13}C concentration higher than the natural value. Such optimization, along with spectral decomposition studies of samples with varying ^{13}C concentrations, at low temperatures and at high magnetic fields, will be pursued in future work. The present results, together with the possibility of single qubit addressability through AFM^{39–41} or super-resolution optical techniques⁴² and intrinsic qubit–qubit interactions¹, pave the way for quantum information, sensing and metrology applications in a robust, multi-qubit solid-state architecture. Finally, the spectral decomposition technique presented here, based on well-known pulse sequences and a simple reconstruction algorithm, can be applied to other composite solid-state spin systems, such as quantum dots and phosphorous donors in silicon. Such measurements could provide a powerful approach for the study of many-body dynamics of complex spin environments, potentially exhibiting non-trivial effects related to the interplay between nuclear and electronic spin baths.

Methods

Single NV confocal microscope. Single NV measurements (HPHT sample) were performed using a custom-built confocal microscope. Optical excitation was provided by a 300 mW 532 nm diode pumped solid-state laser (Changchun New Industries Optoelectronics Tech, MLLIII532-300-1), focused onto the sample using a $\times 100$, NA = 1.3 oil-immersion objective (Nikon CFI Plan Fluor $\times 100$ oil). NV fluorescence was collected through the same optics, and separated from the excitation beam using a dichroic filter (Semrock LM01-552-25). The light was additionally filtered (Semrock LP02-633RS-25) and focused onto a single-photon counting module (Perkin-Elmer, SPCM-ARQH-12). The excitation laser was pulsed by focusing it through an acousto-optic modulator (Isomet 1205C-2).

Microwaves were delivered to the sample through a 20- μm thick wire soldered across it. The wire was driven by an amplified (Mini-circuits ZHL-16W-43-S+) MW synthesizer (Agilent E4428C). Phase modulation of the MW pulses was achieved using an in-phase/quadrature (IQ) mixer (Marki IQ-1545). MW and optical pulses were controlled using a computer-based digital delay generator (SpinCore PulseBlaster ESR400). A static magnetic field of ~ 50 G was applied to the sample to lift the degeneracy of the $m_s = \pm 1$ levels.

NV wide-field fluorescence microscope. NV multi-spin measurements (for samples ^{12}C and Apollo) were performed using a custom-built wide-field fluorescence microscope (Fig. 4a), which has previously been used for two-dimensional magnetic field imaging with thin-layer NV-diamond samples¹³. Optical excitation was provided by a 3-W 532-nm laser (Laser Quantum Opus), which illuminated a large region of interest on the diamond surface through a $\times 20$ NA = 0.75 objective (Nikon). An acousto-optic modulator (Isomet M1133-aQ80 L-H) acted as an optical switch, to pulse the laser with precise timing in order to prepare and detect the NV spin states. A loop antenna was positioned near the diamond surface and connected to the amplified (Mini-circuits ZHL-16W-43-S+) output of a microwave signal generator (Agilent E8257D) to generate a homogeneous B_1 field over the region of interest. Fast-switching of the MW field (ZASWA-2-50DR) enabled coherent manipulation of the NV spin states necessary for coherence decay measurements using CPMG pulse sequences, in order to perform the spectral

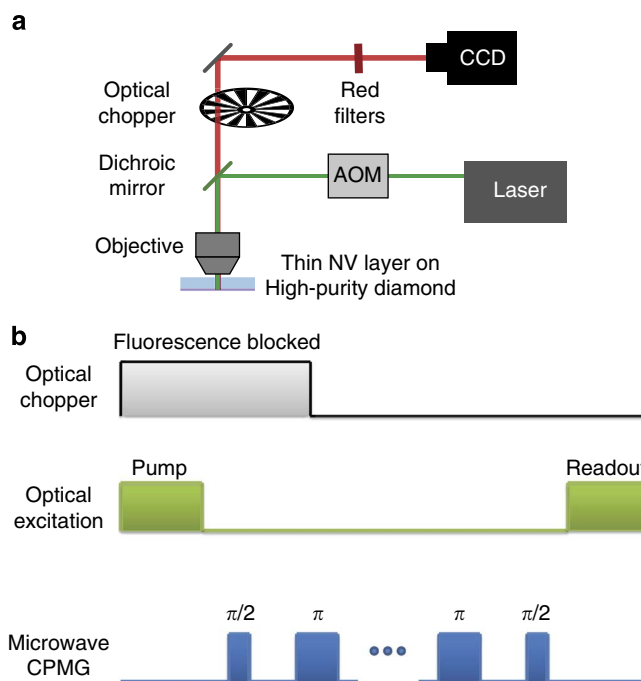


Figure 4 | Details of ensemble measurement setup and pulse sequences.

(a) Diagram of the NV wide-field fluorescence microscope. The laser produces 532-nm light, which is switched by the acousto-optic modulator (AOM) and directed through a dichroic mirror and an objective onto the diamond sample. The fluorescence from the sample passes through the dichroic and, following an optical chopper and appropriate filters, is collected by a charge-coupled device (CCD). (b) Pulse sequence used to perform spectral decomposition measurements with the NV wide-field microscope. Optical pulses are used to first initialize the NV and then to readout its spin state. The optical chopper is synced such that the initialization pulse is blocked from the CCD, while the readout pulse is recorded. The microwave pulses are applied between the initialization and readout optical pulses.

decomposition technique. Optical and MW pulse timings were controlled through a computer-based digital delay generator (SpinCore PulseBlaster PRO ESR500).

NV fluorescence was collected by the objective, filtered, and imaged onto a cooled charge-coupled device camera (Starlight Xpress SXV-H9). As the duration of a single measurement is shorter than the minimum exposure time of the camera, the measurement was repeated for several thousand averages within a single exposure and synchronized to an optical chopper placed before the camera in order to block fluorescence from the optical preparation pulse (Fig. 4b). Repeating the measurement without the MW control pulses provided a reference for long-term drifts in the fluorescence intensity.

In the measurements described here, the loop of wire delivered 3.07 GHz MW pulses to the sample, resonant with the NV $|0\rangle - |1\rangle$ spin transition for the applied static magnetic field ≈ 70 G, to manipulate the NV spin coherence and implement CPMG spin-control pulse sequences.

Spectral decomposition deconvolution procedure. The coherence of a two-level quantum system can be related to the magnitude of the off-diagonal elements of the system's density matrix. Specifically, we deal here with NV electronic spin qubits in a finite external magnetic field, which can be treated as effective two-level spin systems with quantization (z) axis aligned with the NV axis. When the NV spins are placed into a coherent superposition of spin eigenstates, for example, aligned with the x axis of the Bloch sphere, the measurable spin coherence is given by $C(t) = \text{Tr}[\rho(t)S_x]$.

The filter function for the n -pulse CPMG control sequence $F_{\text{CPMG}}(\omega)$ covers a narrow frequency region (given by π/t , where t is total length of the sequence), which is centred at $\omega_0 = \pi n/t$, and is given by⁴³:

$$F_n^{\text{CPMG}}(\omega t) = 8 \sin^2\left(\frac{\omega t}{2}\right) \frac{\sin^4\left(\frac{\omega t}{4n}\right)}{\cos^2\left(\frac{\omega t}{2n}\right)}. \quad (5)$$

We note that the narrow-band feature of the CPMG filter essentially defines the effectiveness of this sequence for dynamical decoupling.

The filter function $F_n^{\text{CPMG}}(\omega t)$ associated with the CPMG pulse sequence deviates from a δ -function by the finite width of the main spectral peak and by the presence of higher harmonics (Supplementary Fig. 1). In addition, the central frequency of the filter function changes with the duration of the experiment and with the number of pulses. Therefore, reconstructing the spin-bath spectral function $S(\omega)$ from the decoherence data requires a solution of the Fredholm type equation to extract $S(\omega)$ equation (1):

$$\chi(t) = \frac{1}{\pi} \int_0^\infty d\omega S(\omega) \frac{F_t(\omega)}{\omega^2}. \quad (6)$$

This extraction is accomplished by assuming that the spectral function decays to zero at high frequency and by noting that the filter function includes high harmonics but negligible low frequency artefacts. Thus, the procedure starts at the high frequency values of $C(\omega)$, and works back to lower frequencies by subtracting the effect of higher harmonics using the reconstructed high frequency values of $S(\omega)$ and the analytical form of the filter function.

Owing to the high frequency components of the filter function and the monotonically decreasing nature of the spectral function, a naive reconstruction of the spectral function assuming a δ -function form of the filter function produces results that are biased to lower values by $\sim 15\%$. This bias is removed using the reconstruction algorithm presented above.

References

- Jiang, L. *et al.* Repetitive readout of a single electronic spin via quantum logic with nuclear spin ancillae. *Science* **326**, 267–272 (2009).
- Neumann, P. *et al.* Single-shot readout of a single nuclear spin. *Science* **329**, 542–544 (2010).
- McCamey, D. R., Van Tol, J., Morley, G. W. & Boehme, C. Electronic spin storage in an electrically readable nuclear spin memory with a lifetime >100 s. *Science* **330**, 1652–1656 (2010).
- Zurek, W. H. Decoherence, einselection, and the quantum origins of the classical. *Rev. Mod. Phys.* **75**, 715–775 (2003).
- Taylor, J. M. *et al.* High-sensitivity diamond magnetometer with nanoscale resolution. *Nat. Phys.* **4**, 810–816 (2008).
- Maze, J. R. *et al.* Nanoscale magnetic sensing with an individual electronic spin in diamond. *Nature* **455**, 644–647 (2008).
- Balasubramanian, G. *et al.* Nanoscale imaging magnetometry with diamond spins under ambient conditions. *Nature* **455**, 648–651 (2008).
- Goldstein, G. *et al.* Environment-assisted precision measurement. *Phys. Rev. Lett.* **106**, 140502 (2011).
- Acosta, V. M. *et al.* Diamonds with a high density of nitrogen-vacancy centers for magnetometry applications. *Phys. Rev. B* **80**, 115202 (2009).
- Childress, L. *et al.* Coherent dynamics of coupled electron and nuclear spin qubits in diamond. *Science* **314**, 281–285 (2006).
- Tyryshkin, A. M., Lyon, S. A., Astashkin, A. V. & Raitsimring, A. M. Electron spin relaxation times of phosphorus donors in silicon. *Phys. Rev. B* **68**, 193207 (2003).
- Hanson, R., Kouwenhoven, L. P., Petta, J. R., Tarucha, S. & Vandersypen, L. M. K. Spins in few-electron quantum dots. *Rev. Mod. Phys.* **79**, 1217–1265 (2007).
- Pham, L. M. *et al.* Magnetic field imaging with nitrogen-vacancy ensembles. *New J. Phys.* **13**, 045021 (2011).
- Stanwix, P. L. *et al.* Coherence of nitrogen-vacancy electronic spin ensembles in diamond. *Phys. Rev. B* **82**, 201201 (2010).
- Allred, J. C., Lyman, R. N., Kornack, T. W. & Romalis, M. V. High-sensitivity atomic magnetometer unaffected by spin-exchange relaxation. *Phys. Rev. Lett.* **89**, 130801 (2002).
- Dobrovitski, V. V., Feiguin, A. E., Awschalom, D. D. & Hanson, R. Decoherence dynamics of a single spin versus spin ensemble. *Phys. Rev. B* **77**, 245212 (2008).
- Barnes, E., Cywinski, L. L. & Das Sarma, S. Master equation approach to the central spin decoherence problem: Uniform coupling model and role of projection operators. *Phys. Rev. B* **84**, 155315 (2011).
- de Lange, G., Wang, Z. H., Rist, D., Dobrovitski, V. V. & Hanson, R. Universal dynamical decoupling of a single solid-state spin from a spin bath. *Science* **330**, 60–63 (2010).
- Naydenov, B. *et al.* Dynamical decoupling of a single-electron spin at room temperature. *Phys. Rev. B* **83**, 081201 (2011).
- Ryan, C. A., Hodges, J. S. & Cory, D. G. Robust decoupling techniques to extend quantum coherence in diamond. *Phys. Rev. Lett.* **105**, 200402 (2010).
- Almog, I. *et al.* Direct measurement of the system environment coupling as a tool for understanding decoherence and dynamical decoupling. *J. Phys. B: Atomic, Mol. Opt. Phys.* **44**, 154006 (2011).
- Bylander, J. *et al.* Noise spectroscopy through dynamical decoupling with a superconducting flux qubit. *Nat. Phys.* **7**, 565–570 (2011).
- Álvarez, G. A. & Suter, D. Measuring the spectrum of colored noise by dynamical decoupling. *Phys. Rev. Lett.* **107**, 230501 (2011).
- Du, J. *et al.* Preserving electron spin coherence in solids by optimal dynamical decoupling. *Nature* **461**, 1265–1268 (2009).
- Klauder, J. R. & Anderson, P. W. Spectral diffusion decay in spin resonance experiments. *Phys. Rev.* **125**, 912–932 (1962).
- Gordon, G., Erez, N. & Kurizki, G. Universal dynamical decoherence control of noisy single- and multi-qubit systems. *J. Phys. B* **40**, S75 (2007).
- Meiboom, S. & Gill, D. Modified spin-echo method for measuring nuclear relaxation times. *Rev. Sci. Instr.* **29**, 688–691 (1958).
- Hahn, E. L. Spin echoes. *Phys. Rev.* **80**, 580–594 (1950).
- Slichter, C. P. *Principles of Magnetic Resonance* (Springer-Verlag, 1990).
- de Sousa, R. Electron spin as a spectrometer of nuclear spin noise and other fluctuations. In: *Electron Spin Resonance and Related Phenomena in Low-Dimensional Structures, of Topics in Applied Physics* (ed. Fanciulli, M.) **115**, 183–220 (2009).
- de Lange, G., Ristè, D., Dobrovitski, V. V. & Hanson, R. Single-spin magnetometry with multipulse sensing sequences. *Phys. Rev. Lett.* **106**, 080802 (2011).
- Medford, J. *et al.* Scaling of dynamical decoupling for spin qubits. *Phys. Rev. Lett.* **108**, 086802 (2012).
- Bloembergen, N. On the interaction of nuclear spins in a crystalline lattice. *Physica* **15**, 386–426 (1949).
- Portis, A. M. Spectral diffusion in magnetic resonance. *Phys. Rev.* **104**, 584–588 (1956).
- de Sousa, R. & Das Sarma, S. Electron spin coherence in semiconductors: considerations for a spin-based solid-state quantum computer architecture. *Phys. Rev. B* **67**, 033301 (2003).
- Witzel, W. M., Carroll, M. S., Morello, A., Cywinski, L. L. & Das Sarma, S. Electron spin decoherence in isotope-enriched silicon. *Phys. Rev. Lett.* **105**, 187602 (2010).
- Cox, A., Newton, M. E. & Baker, J. M. ^{13}C , ^{14}N and ^{15}N endor measurements on the single substitutional nitrogen centre (p1) in diamond. *J. Phys.: Condens. Matter* **6**, 551 (1994).
- Barklie, R. C. & Guven, J. ^{13}C hyperfine structure and relaxation times of the p1 center in diamond. *J. Phys. C* **14**, 3621 (1981).
- Grinolds, M. S. *et al.* Quantum control of proximal spins using nanoscale magnetic resonance imaging. *Nat. Phys.* **7**, 687–692 (2011).
- Arcizet, O. *et al.* A single nitrogen-vacancy defect coupled to a nanomechanical oscillator. *Nat. Phys.* **7**, 879–883 (2011).
- Maletinsky, P. *et al.* A robust scanning diamond sensor for nanoscale imaging with single nitrogen-vacancy centres. *Nat. Nano.* doi:10.1038/nnano.2012.50 (2012).
- Maurer, P. C. *et al.* Far-field optical imaging and manipulation of individual spins with nanoscale resolution. *Nat. Phys.* **6**, 912–918 (2010).
- Cywinski, L. L., Lutchyn, R. M., Nave, C. P. & Das Sarma, S. How to enhance dephasing time in superconducting qubits. *Phys. Rev. B* **77**, 174509 (2008).

Acknowledgements

We gratefully acknowledge fruitful discussions with Patrick Maletinsky and Shimon Kolkowitz; and assistance with samples by Daniel Twitchen and Matthew Markham (Element 6) and Patrick Doering and Robert Linares (Apollo). This work was supported by NIST, NSF, US Army Research Office and DARPA (QuEST and QuASAR programs). PC was partially funded by NSF under grant no. DMG-1005926.

Author contributions

All authors contributed to all aspects of this work.

Additional information

Supplementary Information accompanies this paper at <http://www.nature.com/naturecommunications>

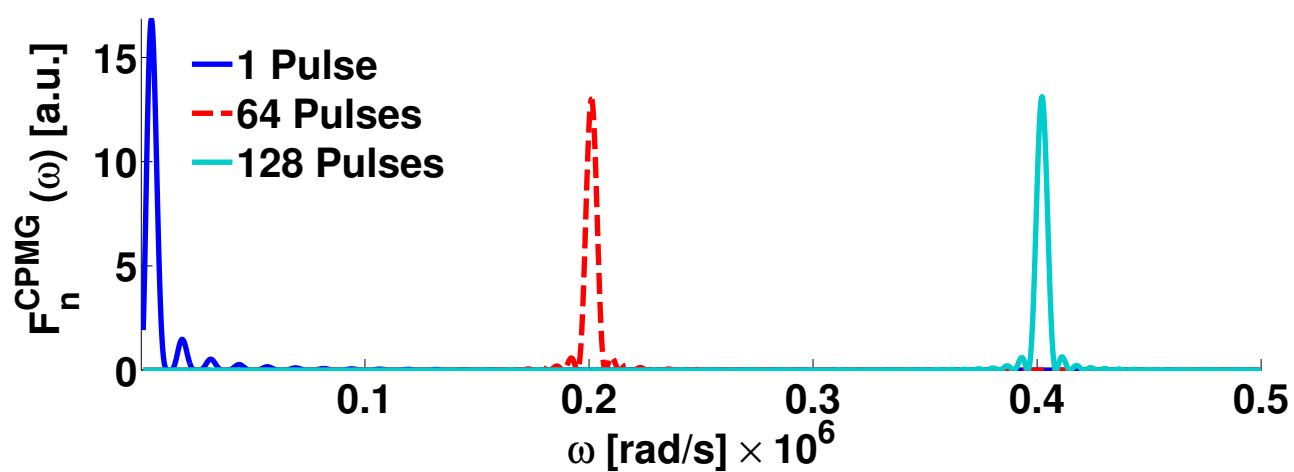
Competing financial interests: The authors declare no competing financial interests.

Reprints and permission information is available online at <http://npg.nature.com/reprintsandpermissions/>

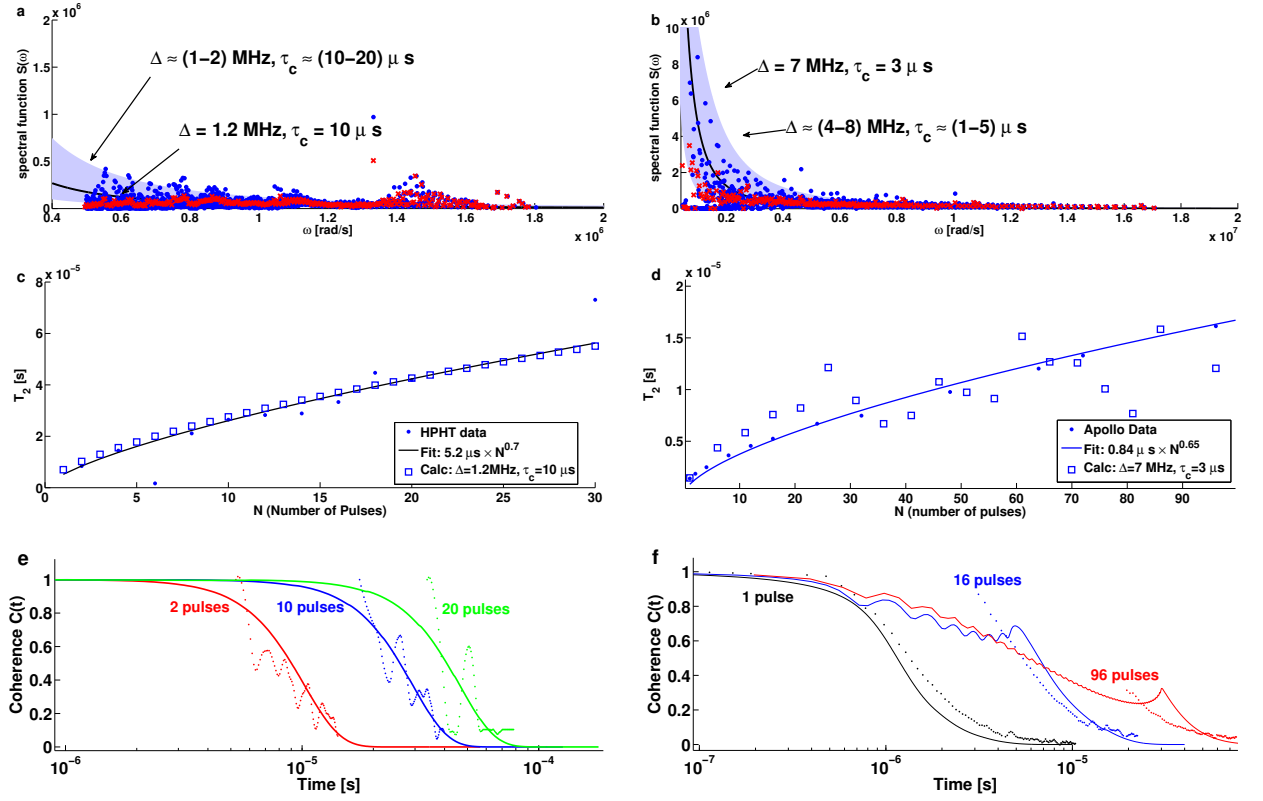
How to cite this article: Bar-Gill, N. *et al.* Suppression of spin-bath dynamics for improved coherence of multi-spin-qubit systems. *Nat. Commun.* **3**:858 doi: 10.1038/ncomms1856 (2012).

Suppression of spin bath dynamics for improved coherence of multi-spin-qubit systems
Supplementary Information

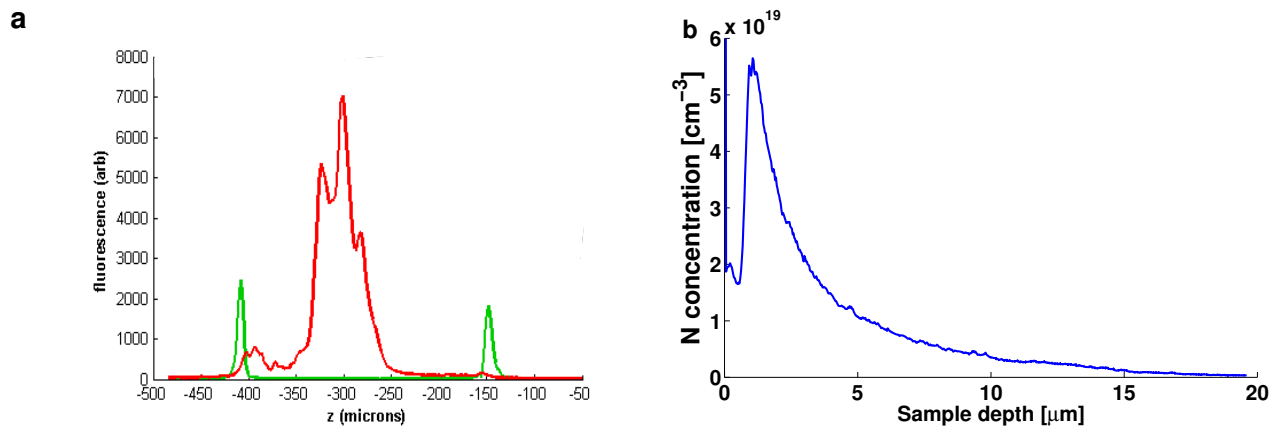
Supplementary Figures



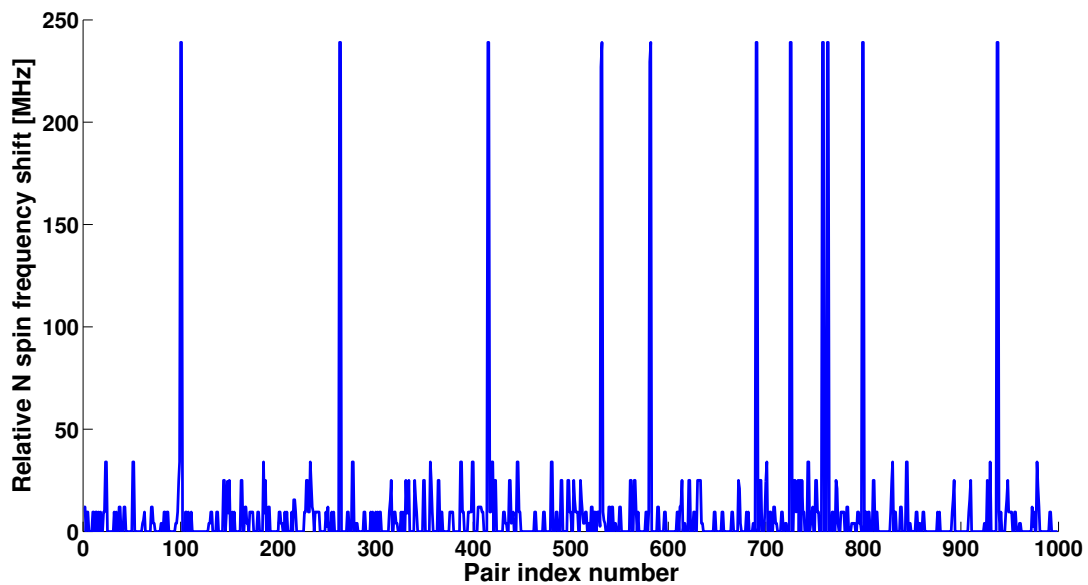
Supplementary Figure S1. CPMG filter functions. Calculated filter function $F_n^{\text{CPMG}}(\omega)$ for three examples of the number n of CPMG pulses ($n = 1, 64, 128$).



Supplementary Figure S2. Spectral analysis of the HPHT (left) and Apollo (right) samples. (a),(b) Derived values for the spin bath spectral functions $S_n(\omega)$ for all CPMG pulse sequences (blue dots) and average values at each frequency (red crosses). Each blue dot represents a pulse sequence with a specific duration t and number of pulses n , such that the probed frequency is $\omega = \pi n/t$. Also shown is the best fit Lorentzian for the mean spectral function $\langle S_n(\omega) \rangle_n$ (solid black line), and a range of best-fit Lorentzians for the individual spectral functions $S_n(\omega)$ for each CPMG pulse sequence (light-blue band). (c),(d) Scaling of T_2 with the number n of CPMG pulses: derived from NV spin coherence decay data $C_n(t)$ (dots); fit of data to a power law (solid line); and synthesized from the average-fit Lorentzian spin bath spectrum (open squares), which yields a consistent fit. (e),(f) Examples of measured NV multi-spin coherence as a function of time $C_n(t)$ for CPMG pulse sequences with different numbers of pulses n (solid lines), and the corresponding synthesized curves calculated using the average-fit Lorentzian spin bath spectrum (dots).



Supplementary Figure S3. Measurements of inhomogeneities in the ^{12}C and Apollo samples. (a) Confocal scan of NV fluorescence and hence concentration (red) as a function of depth in the ^{12}C sample. The green line indicates the surfaces of the sample as measured by enhanced reflection of the green excitation light. (b) Inhomogeneity of N concentration in the Apollo sample as measured using secondary ion mass spectroscopy (SIMS).



Supplementary Figure S4. Monte Carlo simulation of the ^{13}C -induced Overhauser effect. Example results of Monte Carlo simulation of relative frequency shift between 1000 pairs of N electronic spins induced by hyperfine interactions with ^{13}C nuclear spin impurities that are randomly distributed in a diamond lattice at the natural abundance concentration of 1.1%.

Supplementary Methods

Details of spectral analysis For each CPMG pulse sequence (and hence value of n) applied to each sample, we extract the decoherence functional $\chi_n(t) = -\ln C_n(t)$ (see Eq. (1) in the main text) from the relevant NV multi-spin coherence data $C_n(t)$, such as that shown for the ^{12}C sample in Fig. 2a in the main text. The measured coherence $C_n(t)$ is well fit by a stretched exponential $e^{-(t/T_2)^p}$, where the value of p varies between 1 and 3 related to dynamics of the spin environment and ensemble inhomogeneous broadening (see section below on multi-spin averaging). This behavior is consistent with a Lorentzian spin bath spectrum and indicates that N spin impurities are the dominant source of NV spin decoherence. The effects of ^{13}C nuclear spin impurities are discussed in the main text. The second most important electronic spin impurities are NVH defects, which are an order of magnitude less abundant than N impurities [1]. The contribution of instantaneous spin diffusion due to interactions between neighboring NV spins and MW-induced spin flips [2] is also negligible, as the NV Rabi frequency for typical MW power (~ 10 MHz) is large compared to the NV electronic spin transition linewidth (~ 3 MHz), and the NV dipolar coupling timescale (proportional to the inverse of the dipolar coupling energy) is at least an order of magnitude longer than the longest measured NV spin coherence time.

Using the measured $C_n(t)$ data we derive values for the spin bath spectral function $S_n(\omega)$ for each CPMG pulse sequence by deconvolving $\chi_n(\omega)$ with the filter function $F_n^{\text{CPMG}}(\omega t)$ (Supplementary Figure S1). The resulting values for the spectral functions $S_n(\omega)$ for all CPMG pulse sequences (i.e., all values of n) are plotted together in Fig. 2b in the main text. Note that the average data (red crosses) in Fig. 2b in the main text are calculated by binning the full data set for $S_n(\omega)$ into 100 frequency values between 0 and 1 MHz. As a result of this binning procedure, a few data points exhibited abnormally small coherence at low frequency, perhaps due to technical noise, which at ~ 150 kHz contributes two outliers to the averaged data.

We use two methods of analysis to characterize the underlying spin bath spectrum $S(\omega)$ in terms of the coupling strength Δ of the bath spins to the probed NV spins and the correlation time τ_c of the bath spins with each other (Supplementary Figure S2): in the first we separately fit each spectral function $S_n(\omega)$ to a Lorentzian, which provides individual-fit values for Δ and τ_c for each of the CPMG pulse sequences; and in the second we average all the $S_n(\omega)$ values for each ω and then fit the resulting mean spectral function $\langle S_n(\omega) \rangle_n$ to a Lorentzian, which provides single, average-fit values for Δ and τ_c .

The oscillations in the HPHT coherence decay data are a result of a nearby spin impurity (most likely a ^{13}C nuclear spin). The relevant data for the reconstruction of the N-bath spectral function is the envelope of the decay, which was minimally affected by the oscillations.

The coherence decay data for the Apollo sample exhibited some non-monotonic behavior, which was a result of the large coupling strength between NV spins and the spin-bath in this sample, producing semi-coherent interaction effects. These effects were beyond the weak coupling approximation assumed for the spectral decomposition procedure and indicate that higher-order corrections might be non-negligible in this case. However, it can be seen that the second-order theory we employed here for spectral analysis still reproduces the main features of the decoherence curves, as well as the scaling of the NV T_2 with the number of CPMG pulses n .

We note that the frequencies at which the data was taken are dictated by the pulse sequence durations and numbers of pulses and are therefore not always commensurate between different pulse sequences.

We also note that the frequency range of the HPHT data is small compared to the other samples due to: first the short NV spin coherence time, which limits measurement of the very low frequency response; and second the reduced signal-to-noise (as this was a single NV measurement using a confocal apparatus), which limits the measurement of pulse sequences with a large number of pulses, thus excluding very high frequency data.

Multi-spin averaging For measurements with the ^{12}C and Apollo samples, the coherence decay function ($C(t) = e^{-(t/T_2)^p}$) and the scaling of T_2 with the number of CPMG pulses were not fully consistent over all measurement timescales and pulse numbers. This inconsistency was largely a result of averaging over many NV spins in the field of view, which modifies the effective bath spectrum from a simple Lorentzian due to inhomogeneities in the local NV environment and the spin bath. To account for such effects, we used the best average-fit Lorentzian and then calculated the expected coherence decay $C_n(t)$ and scaling of T_2 with CPMG pulse number by averaging over 20 model realizations of the spin-bath spectra, with parameters normally distributed around the values extracted from the average-fit Lorentzian, and the FWHM of this distribution set at 50% of the central extracted values.

The ^{12}C sample (Element 6) is a high quality, pure sample, with a low concentration of N impurities (~ 1 ppm) and a very low concentration of other defects. The sample does not show N-induced steps frequently associated with CVD diamond, due to the low concentration of N in the growth process [3]. The N concentration was calibrated

by Element 6 during growth and then verified to be ~ 1 ppm by bulk EPR measurements. Measurement of N inhomogeneity using SIMS was not possible due to the relatively high N-detection threshold of this method (> 1 ppm). We performed confocal scans of the sample to measure the spatial distribution of NV centers (Supplementary Figure 3(a)), which showed less than a factor of two variation in NV concentration throughout the sample. With the reasonable assumption that N and NV concentrations are proportional to each other, we conclude that the N concentration in this sample is similarly homogeneous to within about a factor of two.

The Apollo sample contains a high concentration of N impurities (~ 100 ppm), which are the dominant source of decoherence for the NV spins. To characterize inhomogeneity of the N concentration, we performed SIMS measurements on this sample (see Supplementary Figure 3(b)). Again assuming the N and NV concentrations are locally proportional to each other, we determined the mean N concentration probed by NV fluorescence measurements, $\overline{n_N}$, from a weighted average over the local N concentration $n_N(z)$:

$$\overline{n_N} = \frac{\int_0^Z dz n_N^2(z)}{\int_0^Z dz n_N(z)}. \quad (\text{S1})$$

Using the SIMS data we find $\overline{n_N} \simeq 2.6(1.7) \times 10^{19} [\text{cm}^{-3}] \simeq 150(100)$ ppm, which is consistent with the coupling strength Δ for this sample extracted using the spectral decomposition technique, with the uncertainties in this value, and with Monte Carlo simulations we performed of the spin environment (see below). In addition, our measurements were carried out on a confined lateral region of $\sim 10 \times 10 \mu\text{m}^2$ to suppress the effects of inhomogeneities on a larger scale. The SIMS measurements also indicate that within the detection limits (1 ppm) there are no other extrinsic defects present, such as Boron or Si.

The HPHT sample also contains a high concentration of N impurities (~ 50 ppm). The low NV density of this sample allowed us to make single NV measurements using a confocal apparatus. Therefore, possible inhomogeneities of the N concentration do not affect the measured data. We measured NV centers in the central region of the HPHT sample, in the 100 growth sector, which was characterized by SIMS to have an N concentration of approximately 50 – 150 ppm, consistent with our spectral decomposition value for the coupling strength Δ .

In summary, for all three samples the values we find for Δ using spectral decomposition are consistent with independent measurements and estimates of the N concentration, which therefore suggests that sample inhomogeneities are within expected ranges and understood to within a factor of 2-3. As a result, we have confidence that the values provided by spectral decomposition for the N spin-bath correlation time τ_c in the HPHT and Apollo samples are an order of magnitude longer than the expected values given by a simple model of the N spin-bath that ignores N- ^{13}C interactions, for the estimated values of N concentration for these two samples.

We note that a long spin-bath correlation time was also measured in an HPHT sample in [4] using a different method than the spectral decomposition technique presented here, further supporting our results. We also note that the results we obtained via spectral decomposition could not be recreated with any combination of Δ and τ_c that follow the expected scaling with N concentration, regardless of the actual value of the assumed concentration and including inhomogeneous effects. Therefore, the combined results from the three samples, along with the independent measurements and estimates of N concentration and inhomogeneity, and the consistency of the extracted values for Δ , strongly support the validity of the unexpectedly long correlation time τ_c observed in the HPHT and Apollo samples.

Lorentzian parameters for an N dominated bath For the samples measured in this work, N electronic spins (P1 centers) are the dominant environment coupling to NV spins. Thus, the expected parameters of the Lorentzian bath spectra can be derived from electronic dipolar interactions. The dipolar interaction energy between electronic spins is given by $U_{\text{dip}} \approx \alpha n_N$, where $\alpha \approx 3.3 \times 10^{-13} \text{ s}^{-1} \text{ cm}^3$ and n_N is the N concentration [5]. Therefore the parameters of the Lorentzian spectrum are estimated to be $\Delta \approx U_{\text{dip}}$ and $\tau_c \approx 1/U_{\text{dip}}$.

^{13}C induced broadening of N spin resonance Inhomogeneous broadening of an ensemble of N electron spin resonances in diamond due to proximal ^{13}C nuclear spin impurities is dominated by the strong N- ^{13}C contact hyperfine interaction (compared to the weaker dipolar contribution, see [6, 7]). Therefore, the inhomogeneous broadening energy ΔE does not scale simply with the concentration of ^{13}C . To make a realistic estimate of ΔE , we carried out a Monte-Carlo simulation of 1000 pairs of N spin impurities, each with a different random distribution of ^{13}C spin impurities in a diamond lattice at their natural abundance of 1.1%. The calculated relative electronic spin resonance frequency shift for each N pair is plotted in Supplementary Figure S4. We find the average value of this detuning ≈ 9.5 MHz and the standard deviation ≈ 30 MHz, with a few rare events in which a ^{13}C occupies the nearest lattice to the N, producing a frequency shift ~ 300 MHz. We conclude from this simulation that $\Delta E \sim 10$ MHz, which is consistent with the suppression of N spin bath dynamics revealed by the spectral decomposition measurements and analysis.

Classes of P1 centers in diamond The electronic wavefunction of the P1 center (N impurity in the present case) is anisotropic and can be directed along each of the nearest C bonds. Therefore, there are generally 4 different classes of P1 centers. With a static magnetic field aligned along one of the axes, the hyperfine interaction separates the P1 center's electronic spin resonance into 5 different energies, depending on the class of P1 center (aligned with magnetic field or not) and the N nuclear spin state. This splitting is expected to suppress electronic spin flip-flops between P1 centers with different resonance energies. However, since this effect should be equally manifest in all samples regardless of the concentration of ^{13}C impurities, and since it can maximally account for a factor of 5 change, we conclude that it is not the dominant mechanism underlying the observed order-of-magnitude increase in the correlation time of the electronic spin bath in the presence of finite nuclear spin impurity concentration, as described in the main text.

-
- [1] Edmonds, A. M. *et al.* Production of oriented nitrogen-vacancy color centers in synthetic diamond. *ArXiv e-prints* (2011). 1112.5757.
 - [2] Salikhov, K., Dzuba, S. & Raitisimring, A. The theory of electron spin-echo signal decay resulting from dipole-dipole interactions between paramagnetic centers in solids. *Journal of Magnetic Resonance (1969)* **42**, 255 – 276 (1981).
 - [3] Martineau, P. M. *et al.* Identification of Synthetic Diamond Grown Using Chemical Vapor Deposition (CVD). *Gems & Gemology* **40**, 2–25 (2004).
 - [4] de Lange, G. *et al.* Controlling the quantum dynamics of a mesoscopic spin bath in diamond. *Arxiv*: 1104.4648v1 (2011).
 - [5] Taylor, J. M. *et al.* High-sensitivity diamond magnetometer with nanoscale resolution. *Nat. Phys.* **4**, 810–816 (2008).
 - [6] Cox, A., Newton, M. E. & Baker, J. M. ^{13}C , ^{14}N and ^{15}N endor measurements on the single substitutional nitrogen centre (p1) in diamond. *Journal of Physics: Condensed Matter* **6**, 551 (1994).
 - [7] Barklie, R. C. & Guven, J. ^{13}C hyperfine structure and relaxation times of the p1 center in diamond. *J. Phys. C* **14**, 3621 (1981).